05

Electrophysical properties of titanium dioxide microscrolls doped with linear carbon chains stabilized by gold nanoparticles

© D.N. Bukharov, A.F. Lelekova, V.D. Samyshkin, N.A. Khalimov, S.P. Eyum Ssaka, A.A. Kuznetsov, D.A. Bodunov, A.S. Abramov, A.O. Kucherik

Vladimir State University,
Vladimir, Russia

e-mail: buharovdn@gmail.com

Received September 09, 2024
Revised October 18, 2024
Accepted October 21, 2024

A three-stage method for the synthesis of a system of titanium dioxide microswitches witha periodic structure is proposed: deposition of a porous film by laser ablation, alloying it with linear carbon chains stabilized with gold nanoparticles by Spraying-Jet, and formation of microswitches by the blading method. The structure of the obtained samples was studied, the sizes of the forming elements were estimated, their dendritic structure and periodic character were shown. The study of the electrophysical properties of a system of dioxide micro-coils has been carried out titanium doped with carbon chains fixed between gold nanoparticles during the excitation of a photocurrent in them, which demonstrated the photovoltaic properties of the obtained samples. Varying the excitation parameters of the photocurrent (radiation power and irradiation time) made it possible to achieve quantum efficiency up to values of the order of 29% and 46%, respectively. A model in the Schottky diode approximation is proposed to describe the volt-ampere characteristics of the studied microswitch systems and the photocurrent in them with a relative error of no more than 10%. A comparison with similar systems has been carried out, alloyed metal-carbon complexes based on copper and iron nanoparticles, which demonstrated that they can act as an alternative to complexes with gold nanoparticles.

Keywords: titanium dioxide microgrids, optical excitation, photocurrent, Schottky diode model.

DOI: 10.61011/EOS.2024.10.60056.7059-24

1. Introduction

Micro- and nanostructures based on titanium dioxide (TiO_2) are currently regarded as promising innovative materials and, owing to their unique operational and physical characteristics, are being studied extensively in the context of various applications [1]. For example, TiO_2 nanotubes are used as solid-state components for the development of highly efficient photocatalytic elements, solar cells, sensor and photochromic devices, and coatings for biomedical implants and have many other high-tech applications [2–4]. TiO_2 nanofilms offer fine photosensitivity, chemical and mechanical stability, and unique optical properties [5,6]. In addition, depending on the degree of oxidation, they manifest mixed electrophysical properties and may enhance their capacity to conduct electric current due to a high density of surface defects and the emergence of photocurrent under surface irradiation [7,8]. Their high refraction index also makes them promising components for various optical applications.

A wide range of methods for synthesizing titanium dioxide micro- and nanotubes is currently available. Among them are, e.g., hydrothermal synthesis, which allows one to obtain samples with a diameter of $10-30$ nm and a length of $100-300$ nm [9], and electrochemical synthesis by anodic oxidation, which enables the synthesis of samples with lengths varying from 550 nm to 1.5 μm and diameters ranging from 42 to 53 nm [1]. Common techniques for synthesis of such structures typically require significant time and conditions that are relatively hard to maintain (e.g., high temperature and pressure).

A three-stage procedure [10] based on laser synthesis of a porous titanium dioxide film with subsequent mechanical formation of microscroll systems may be regarded as a simple alternative that does not impose such strict synthesis conditions and allows one to produce extended micro- and nanotube samples with an ordered structure and promising photoelectric properties in a relatively short time. The indicated synthesis method, which was used in the present study to form microstructures doped with linear carbon chains and gold nanoparticles, is characterized in Section 2. The results of examination of structural features of such samples, which are presented in Section 3, reveal their periodic nature. The estimates of their electrophysical and photoelectric properties based on the volt–ampere characteristics (VACs) and quantum efficiency (see Section 4) are in line with the results of modeling based on the Schottky diode approximation (Section 5).

Thus, the aim of the present study is to demonstrate the emergence of well-pronounced promising photoelectric properties in titanium dioxide microscroll structures fabricated via three-stage synthesis.

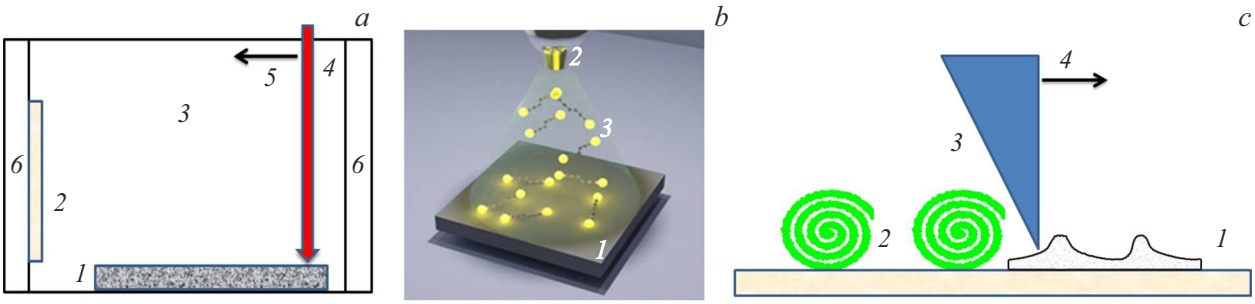

Figure 1. Diagram of synthesis of titanium dioxide microscrolls. (*a*) Synthesis of the TiO_2 structure: *1* — target, *2* — ITO glass substrate, *3* — working chamber, *4* — laser radiation, *5* — direction of motion, and *6* — magnets; (*b*) C-Au spraying into the TiO_2 structure: *1* — substrate, *2* — spray nozzle, and *3* — linear carbon chains stabilized by gold nanoparticles; (*c*) rolling of microscrolls: *1* — TiO_2 porous film with C-Au, *2* — microscrolls, *3* — blade, and *4* — direction of motion.

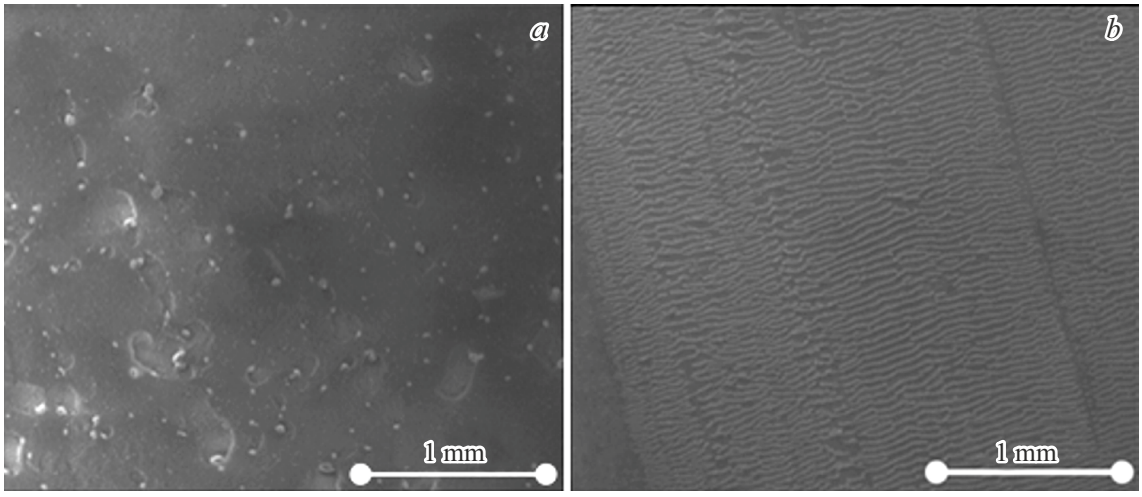

Figure 2. SEM images of the sample surface: *a* — image of the initial TiO_2 film prior to rolling into scrolls; *b* — array of TiO_2 microtubes obtained as a result of mechanical blading.

2. Description of the experimental synthesis procedure

At the first stage of the experiment on synthesis of titanium dioxide microscrolls, a thin porous titanium dioxide film was applied to a substrate made of glass coated with indium tin oxide (ITO glass). Standard ITO glass $20 \times 20 \times 1.1$ mm in size with a sheet resistance of 7–10 Ohm/sq, an ITO film thickness of 200 ± 50 nm, and an ITO layer roughness of 3 nm was used. A titanium dioxide film was synthesized by laser ablation in air (Fig. 1, *a*) from a titanium target (with a purity of 99.99%) 1×1 cm in size. The target was irradiated by an LDesigner F1 laser system operating at a power level of 10 W and a wavelength of 1.06 μm. This laser irradiation was performed in the pulse mode with a frequency of 20 kHz and a pulse duration of 100 ns. The working area was scanned with a beam 30 μm in diameter at a rate of 15 mm/s. After 9 min of irradiation of the initial material, a TiO_2 film with an average thickness of 4 μm and a non-uniform relief was formed on the substrate.

To improve the optical and electrophysical properties of the sample, the Spraying-Jet method was used at the second stage to spray linear carbon chains stabilized by gold nanoparticles [11] into the porous titanium dioxide film matrix.

This was done with an experimental setup allowing one to spray a colloidal solution under pressure through a nozzle onto the surface of the titanium dioxide matrix (Fig. 1, *b*). The colloidal C-Au (carbon-gold) solution was obtained from a solution of shungite with added gold nanoparticles in alcohol. The laser fragmentation method detailed in [12] was used in preparation of this solution.

As was demonstrated in earlier experiments, metal-carbon complexes based on linear carbon stabilized by gold nanoparticles are capable of producing a significant number of photoexcited electrons [11].

At the third stage, an array of microtubes (scrolls) was formed by blading (i.e., through mechanical impact exerted on the TiO_2 film by a blade moving along a given trajectory; see Fig. 1, *c*) from the TiO_2 film to create a metasurface with an increased light absorption coefficient.

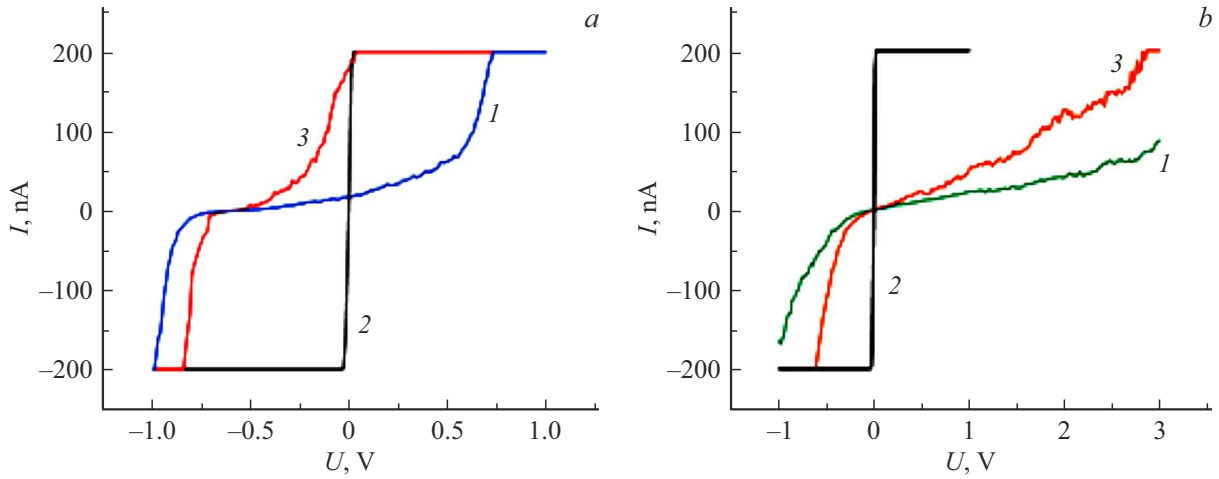

Figure 3. VACs of the sample with the microscroll system measured at an arbitrary point: *1* — without irradiation, *2* — ITO glass, and *3* — with irradiation; the measurement environment is air (*a*) and vacuum (*b*).

In our view, this method is more technologically advanced than the previously proposed technique of metasurface formation in the process of ablation in a magnetic field [13].

3. Examination of structural features of the obtained samples

Samples of titanium dioxide microscrolls with the diameter of elements depending on the distance between the blade and the substrate surface were prepared in accordance with the above procedure. A distance on the order of $9\,\mu$m, which corresponded to the average outer microscroll radius, was set. SEM images of the obtained samples revealed that microscrolls form arrays with elements featuring a branched dendritic structure (Fig. 2). To prove this assumption, the fractal dimension of the sample from Fig. 2 was estimated using the boxcounting [14] method implemented in MATLAB. The obtained value (1.74) corresponds to a dendritic structure.

The average diameter of microscrolls in the sample from Fig. 2 was $9\,\mu$m, the maximum length of the array elements was $225\,\mu$m, and the distances between the microscrolls and their branches fell within the range from 32 to $254\,\mu$m. The values were estimated with a relative error no greater than 9%. The distance between the system elements varied about the value of $37\,\mu$m, deviating by 10–15% from it. In addition, microscrolls had the same average degree of branching with respect to long branches and the same fractal dimension within the 1.74–1.79 interval. All this indicated that the synthesized system of microscrolls had a periodic nature.

4. Study of electrophysical properties

The VACs of samples were measured using an Ntegra Aura atomic force microscope in the semi-contact tunnel current measurement mode. Two distinct measurement scenarios were implemented: in the first case, the VACs were estimated without optical pumping; in the second case, the VACs with photocurrent were recorded under external irradiation by an LCS-T-11 laser source with wavelength $\lambda = 532$ nm, power $P = 8$ mW, and a beam diameter of 3 mm.

The sample with the microscroll system was examined by AFM both in a natural environment (in air) and in vacuum. This allowed us to record the VAC of tunnel current from its surface. Figure 3 shows the results of VAC measurement at a single point in air (panel *a*) and in vacuum (panel *b*).

Thus, it was demonstrated that the VACs of the sample with the microscroll system correspond to a semiconductor material, while the plots for ITO glass reveal metallic conductivity.

A significant difference between the VACs recorded in vacuum and in air is seen in Fig. 3. This may be attributed to the presence of free electrons, which enhance the tunnel current, in the natural atmosphere directly under the needle. Also, zero current is observed at zero voltage only in vacuum, which is illustrative of electron emission. In air, it is recorded at a negative voltage due to the emergence of an additional charge on the surface. However, an increase in current after the introduction of laser pumping at the same voltage level was noted in all measurements. This is indicative of photosensitivity of the examined material and the external photoelectric effect.

VAC measurements were performed at ten different points for the purpose of averaging. The averaged plots are shown in Fig. 4. Figure 4, *a* shows an estimate of the VAC in vacuum without optical pumping.

Figure 4, *b* presents the VAC estimate averaged over ten points in vacuum with account for the effect of pumping radiation. Figure 4, *c* shows the VAC of photocurrent (the difference between the current values in Figs. 4, *b* and *a*: $I_f = I_t - I_l$, where I_t is the current without irradiation and I_l is the current after irradiation). It is evident from

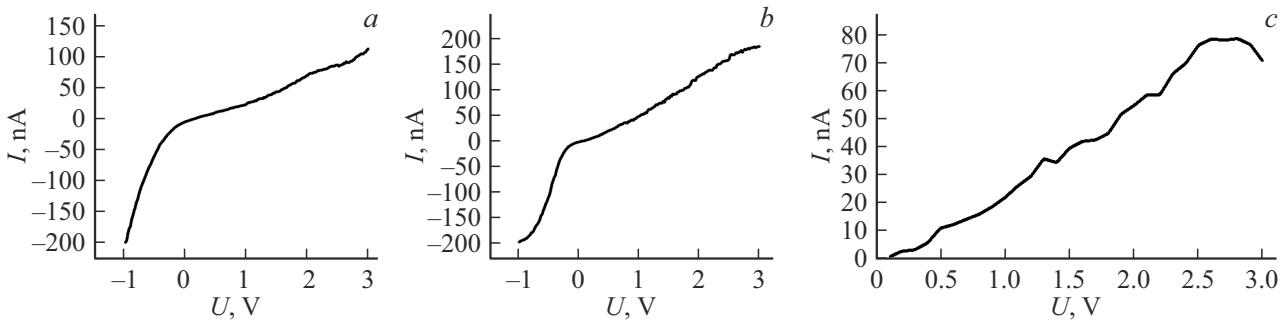

Figure 4. VACs measured in vacuum without (a) and with (b) irradiation by a green laser; VACs of photocurrent of the positive branch (c).

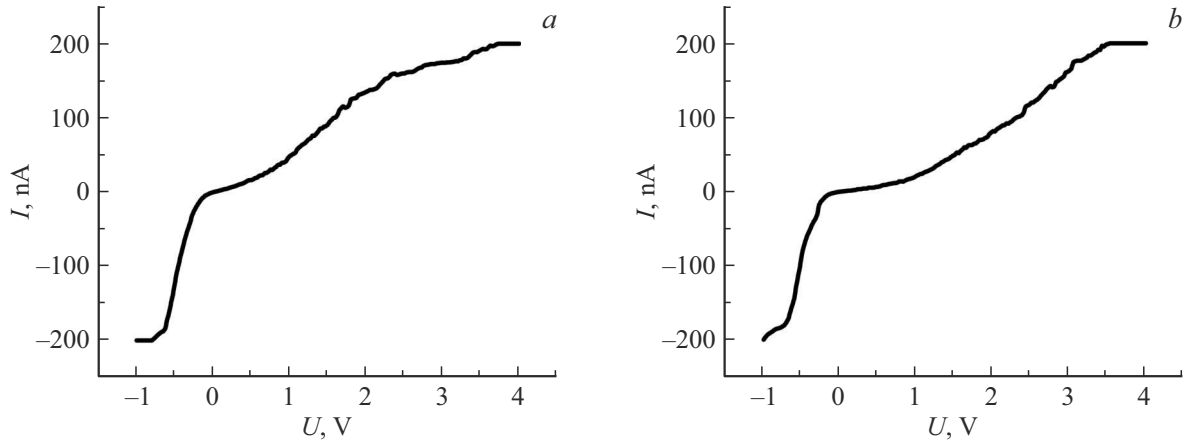

Figure 5. VACs in air: without (a) and with (b) irradiation.

Fig. 4, c that the obtained dependence behaves like a typical photocurrent VAC.

Figure 5 shows the VACs measured in air. Figure 5, a shows the VACs without laser irradiation, while Fig. 5, b presents the characteristics obtained with external pumping.

The quantum efficiency estimate for VAC measurements performed in a given surface region is on the order of 0.9%.

It follows from Figs. 4 and 5 that the obtained dependences are exponential in nature. The saturation currents for VAC branches with positive voltage in air are relatively equal. In the case of measurements in vacuum, they differ significantly. This VAC feature is typical of materials with fairly pronounced photoelectric properties.

To record the photocurrent from the entire test sample surface, an experimental circuit presented in Fig. 6, a, where the sample is depicted as resistor $R1$, was devised. The photocurrent was measured with a Fluke 289 multimeter.

The first measurement was performed for a sample with a TiO_2 film; in the second experiment, the photocurrent after deposition of a colloidal C-Au solution was estimated; in the third measurement, the photocurrent after rolling of the scrolls was investigated. External pumping was implemented in accordance with the diagram shown in Fig. 6, b, which allowed us to focus laser radiation with wavelength $\lambda = 532\,\text{nm}$ onto the surface of a mirror that redirected this radiation onto the surface of the sample. The mirror was used to extend the laser path.

The initial surface of the sample with the TiO_2 film had an electric resistance on the order of $R = 600\,\text{Ohm}$. When voltage $U = 8\,\text{V}$ was applied from a DC power source, current I reached the level of 21 mA. The current flowing through the sample remained unchanged under laser irradiation, indicating the lack of a photoelectric effect.

Following spraying of the colloidal solution containing linear carbon stabilized by gold nanoparticles onto the TiO_2 film surface, the resistance decreased to 545 Ohm. When voltage $U = 8\,\text{V}$ was applied to the sample, current $I = 28.9\,\text{mA}$ flowed through it. When the sample surface was pumped with laser radiation for 30 s, a small increase in current (to $I = 29.03\,\text{mA}$) was recorded. Photocurrent $I_{\text{ph}} = 0.13\,\text{mA}$ was calculated at this stage. The quantum efficiency estimate for this intermediate sample, which was calculated as $\eta \sim \frac{I_{\text{ph}}}{q\Phi}$ [15] (Φ is the luminous flux), was found to be on the order of 2.5%.

Following the formation of microscrolls from the film doped with stabilized linear carbon chains, the measured sample resistance increased to $R = 640\,\text{Ohm}$. When voltage $U = 8\,\text{V}$ was applied to the sample from the external power source, the current in the circuit was $I = 26.38\,\text{mA}$. When

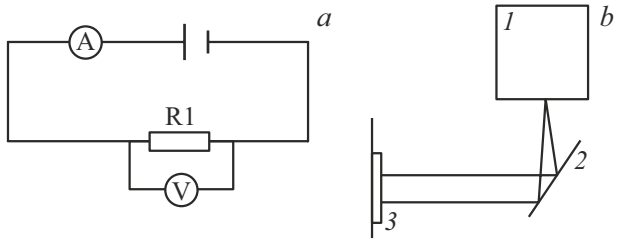

Figure 6. Photocurrent measurement diagrams. Circuit diagram (*a*) and diagram of laser pumping of the sample surface: *1* — laser radiation source, *2* — mirror, and *3* — sample (*b*).

the sample was exposed to laser radiation with wavelength $\lambda = 532\,\text{nm}$, power $P = 1.165\,\text{W}$, and beam diameter $D = 11\,\text{mm}$ for 30 s, the current in the circuit increased to $I = 26.58\,\text{mA}$. Thus, the photocurrent was $I_{\text{ph}} = 0.2\,\text{mA}$. The estimated quantum efficiency for the entire sample was close to 3.8%. Thus, it can be concluded that the sample in its final form had slightly more pronounced photoelectric properties than the original structure.

Figure 7 shows the dependence of current strength on irradiation parameters in the case of exposure of the sample surface to a beam of green light at an electric voltage of 8 V. The estimated dependence of current on the irradiation source power is presented in Fig. 7, *a*. Figure 7, *b* presents the dependence of current on the time of irradiation with green light with a power of 300 mW. The power dependences of current were exponential in nature. The dependence of current on the irradiation time was logarithmic.

A quantum efficiency around 29% may be achieved by raising the radiation source power to 800 mW, and an efficiency of 46.2% is obtained by extending the exposure time at $P = 8\,\text{mW}$.

For comparison purposes, the dependences of current strength on power and irradiation time were examined at an electric voltage of 8 V for samples in which chain carbon was stabilized by copper (Cu; Fig. 9) and iron (Fe; Fig. 8) nanoparticles. If the sample was doped with copper nanoparticles, the current strength started increasing only at a power of 400 mW. However, it reached higher values, but at a much lower rate than in the sample doped with gold. The dependence of current strength on irradiation time was near-linear. A similar effect was found in the iron-doped sample.

A comparison of Figs. 8, *a, c* and 7, *a* reveals a significant reduction of the current strength in its dependence on irradiation power: the values for the sample with Fe nanoparticles are approximately 10 times lower, while the current for the sample with Au nanoparticles is 1.5 times lower than the corresponding values for Cu nanoparticles. At the same time, compared to the samples with Cu and Fe nanoparticles, the current strength in the sample with Au nanoparticles increases at a higher rate. In addition, the maximum growth of current in the dependence on irradiation time is also found in the sample with Au nanoparticles. Specifically, the maximum value of current in its dependence on irradiation time for the sample with Au doping is 1.39 times higher than the corresponding value for the sample with Cu nanoparticles and 1.25 times higher than in the sample with Fe nanoparticles. Comparing Figs. 8, *b* and *d*, which show the time dependences plotted with an error of $0.005\,\mu\text{A}$, one sees clearly that the maximum values of current in its dependence on irradiation time for the samples with Fe and Cu nanoparticles are quite close (the estimated ratio of the corresponding average values is just 1.054). Thus, is follows from a comparison of Figs. 7 and 8 that samples with Fe and Cu nanoparticles may be a fine alternative to Au-doped structures. Moreover, the sample with Cu nanoparticles may have a slightly higher quantum efficiency than the Au-doped sample. For example, if one compares Figs. 7, *a* and 8, *a*, the sample with Cu nanoparticles has an estimated 1.5-fold advantage in quantum efficiency over the sample with Au doping. It should be noted that no changes in surface relief were recorded after laser pumping; i.e., the impact did not lead to destruction of the samples.

5. Simulation of electrophysical properties

Since the structures under consideration feature a metal–semiconductor contact (TiO_2-Au-C(n)-Au-TiO_2), a Schottky barrier will form at the points of contact of gold nanoparticles with the titanium dioxide matrix [15–17].

The simulation was carried out for positive polarity at $U > 0$; VACs were characterized in the Schottky diode approximation [17]:

$$I_d = I_s\left(\exp\left(\frac{|q|U}{NkT}\right) - 1\right)\epsilon,$$

where I_s is the saturation current, k is the Boltzmann constant, T is temperature, q is the electron charge, N is the ideality factor, and ϵ is the proportionality coefficient depending on the contact area and the electron scattering coefficient.

The Schottky diode parameters were estimated from the VAC measured experimentally within the voltage range of $[0.3; \varphi_b]$, where φ_b is the Schottky barrier height. The VAC values averaged over ten measurements taken from Fig. 4, *a* within the positive voltage range of $[0.3; 1.3]\,\text{V}$ were used for modeling.

The ideality factor was estimated as [18]

$$N = \frac{|q|}{bkT},$$

where b is the slope ratio of the linear VAC approximation (I_l).

The extrapolated value of

$$\ln(I/I_s) = \frac{|q|}{U/NkT}$$

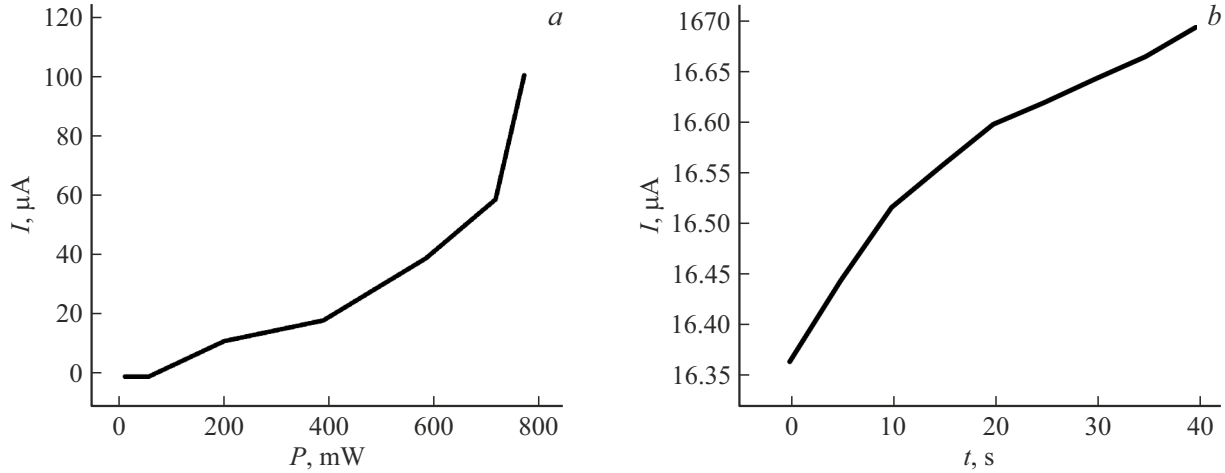

Figure 7. Dependences of current strength at an electric voltage of 8 W on irradiation parameters: *a* — power of the irradiating source; *b* — time of irradiation with green light with a power of 300 mW.

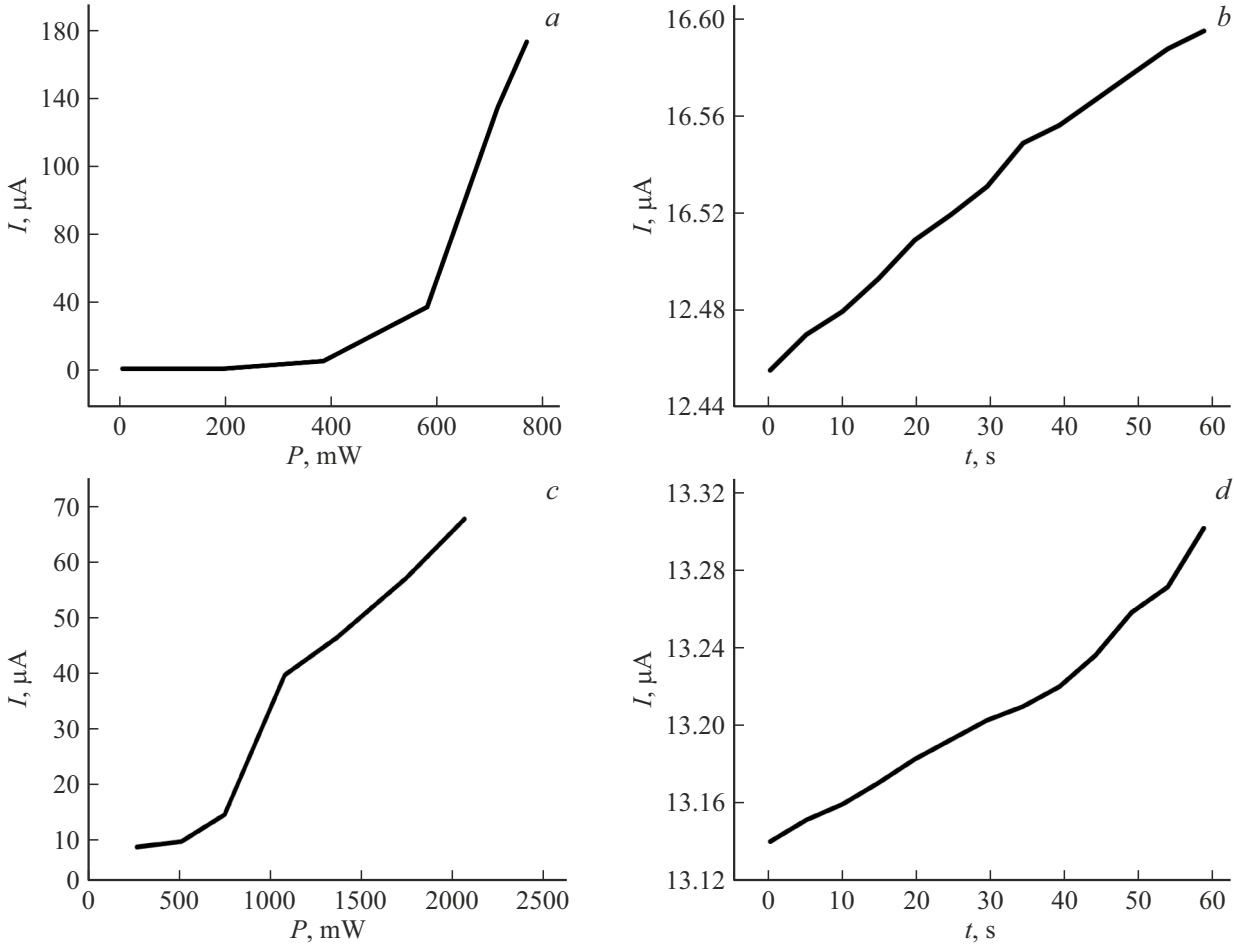

Figure 8. Study of the dependence of current strength *a* — on the radiation source power in the case of doping with Cu nanoparticles; *b* — on the irradiation time for the sample with Cu nanoparticles; *c* — on the radiation source power for the sample with Fe nanoparticles; and *d* — on the irradiation time for the sample with Fe nanoparticles.

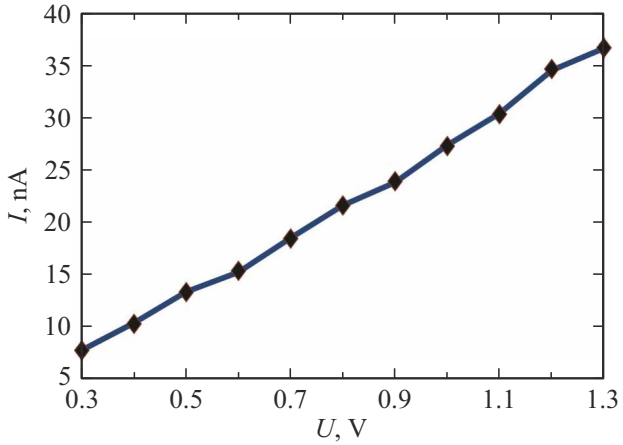

Figure 9. VAC model in the Schottky diode approximation.

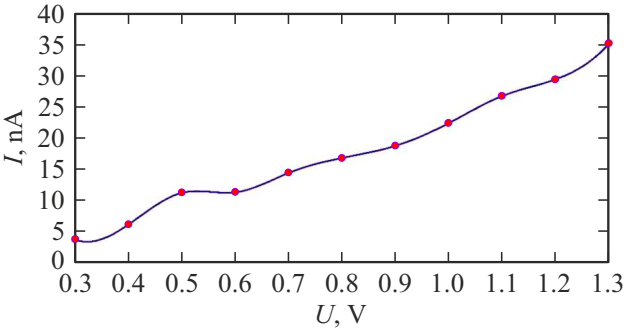

Figure 10. Model of the photocurrent VAC from Fig. 4, *c* with smoothing by splines.

at point $U = 0$ provided an opportunity to estimate the saturation current as $I_l(0) = I_s$. The Schottky barrier height was estimated as [19]

$$\varphi_b = \ln\left(\frac{A^* T^2}{I_s}\right)\frac{NkT}{|q|}.$$

Thus, the following parameters needed for calculations were determined for the VAC from Fig. 4, *a*: $N = 1.242$, $I_s = 23.4$ nA, and $\varphi_b = 1.347$ eV. The model VAC shown in Fig. 9 was plotted with the specified parameters. The maximum difference between the model and experimentally measured values did not exceed 0.13 nA, which is indicative of fine accuracy of the model approximation.

The photocurrent VAC values averaged over ten measurements under irradiation with a laser with a wavelength of 532 nm taken from Figs. 4, *b, c* within the positive voltage range of $[0.3; 1.3]$ V were used as data for modeling and comparison of calculated and experimental results.

The photocurrent was modeled based on the following relation [20]:

$$I_{\text{ph}} = \frac{qF\mu\tau}{d^2}\gamma,$$

where $F = \sqrt{2qU/m_e}$ — velocity of free electrons, $\mu = F * U/d$ — mobility, d — film–probe distance (0.1 nm), m_e — electron mass, τ — lifetime (10^{-10} s), and γ — level of illumination. Figure 10 shows the calculated photocurrent VAC with spline smoothing.

The maximum relative error of the model did not exceed 5%, which is indicative of fine accuracy of the model approximation.

The modeling data do not contradict the results of actual experiments. Thus, we have proposed a fairly simple model with a small number of parameters that provides a fairly adequate description of the electrophysical properties of real samples. This model approach may be used as a first approximation for characterizing the electrophysical properties of real samples.

6. Conclusion

The proposed method for fabrication of titanium dioxide microscrolls opens the way to simple and convenient production of ordered samples that does not require complex synthesis conditions. The synthesized microscroll systems have a dendritic structure with a small degree of branching. The results of experiments and modeling of the electrophysical properties of such microscrolls doped with metal-carbon complexes stabilized by gold nanoparticles revealed their promising photoelectric properties. This is confirmed by fairly high values of quantum efficiency, which reaches 46% and may be adjusted by varying the pumping parameters (duration and power). The comparison of electrophysical properties of samples with Au nanoparticles and similar systems doped with Cu and Fe nanoparticles demonstrated that the latter may serve as a fine alternative, providing both stabilization of linear circuits and enhancement of photocurrent.

Thus, samples synthesized on ITO glass substrates open up new opportunities for photovoltaic applications (e.g., the production of transparent solar cells).

Funding

This study was supported financially by the Russian Science Foundation, grant No. 23-29-10016.

Conflict of interest

The authors declare that they have no conflict of interest.

References

[1] A.A. Rempel, A.A. Valeeva, A.S. Vokhmintsev, I.A. Weinstein. Chem. Rev., **90** (11), 1397 (2021).

[2] F. Heidenau, W. Mittelmeier, R. Detsch, M. Haenle, F. Stenzel, G. Ziegler, H. Gollwitzer. J. Materials Science: Materials in Medicine, **16** (10), 883–888 (2005). DOI: 10.1007/s10856-005-4422-3

[3] I.B. Dorosheva, A.S. Vokhmintsev, I.A. Weinstein, A.A. Rempel. Phys. Chem. Math., **14** (4), 447–453 (2023). DOI: 10.17586/2220-8054-2023-14-4-447-453

[4] T.C. Selema, T.D. Malevu, M.R. Mhlongo, S.V. Motloung, T.E. Motaung. Eemergent Mater, (2024). DOI: 10.1007/s42247-024-00731-z
[5] A.A. Hendi, M.M. Alanazi, W. Alharbi, T. Ali, M.A. Awad, K.M. Ortashi, H. Aldosari, F.S. Alfaifi, R. Qindeel, G. Naz, T.H. Alsheddi. J. King Saud University — Science, **35** (3), 1–7 (2023). DOI: 10.1016/j.jksus.2023.102555
[6] D.K. Njoroge. Sci. Tech. Energ. Transition, **78**, 26 (2023). DOI: 10.2516/stet/2023024
[7] Z. Zhao, X. Zhang, G. Zhang et al. Nano Res., **8**, 4061–4071 (2015). DOI: 10.1007/s12274-015-0917-5
[8] Z. Barlow, Z. Wei, R. Wang. Materials Chemistry and Physics, **309**, 128316 (2023). DOI: 10.1016/j.matchemphys.2023.128316
[9] Y.G. Guo, L.J. Wan, C.L. Bai. J. Phys. Chem. B, **107** (1), 5441–5444 (2003).
[10] S. Kavokina, V. Samyshkin, J. Cao, A. Abramov, A. Osipov, S.P. Essaka, N. Khalimov, D. Bodunov, A. Kavokin. Nanomaterials, **14** (1), 56 (2024). DOI: 10.3390/nano14010056
[11] S. Kutrovskaya, I. Chestnov, A. Osipov, V. Samyshkin, I. Sapegina, A. Kavokin, A. Kucherik. Scientific Reports, **10** (1), 9709 (2020). DOI: 10.1038/s41598-020-65356-8/
[12] A.O. Kucherik, S.M. Arakelian, S.V. Garnov, S.V. Kutrovskaya, D.S. Nogtev, A.V. Osipov, K.S. Khor'kov. Quantum Electronics, **46** (7), 627 (2016). DOI: 10.1070/QEL16128
[13] V. Samyshkin, A. Lelekova, A. Osipov, D. Bukharov, I. Skryabin, S. Arakelian, S. Kutrovskaya. Optical and Quantum Electronics, **51** (1), 1–9 (2019). DOI: 10.1007/s11082-019-2114-3
[14] S. Kutrovskaya, A. Kucherik, A. Osipov, V. Samyshkin, A. Istratov, A.V. Kavokin. Scientific Reports, **9** (1), 1–9 (2019). DOI: 10.1038/s41598-019-43588-7
[15] G.A. Gonzato. Computers & Geosciences, **24** (1), 95–100 (1998). DOI: 10.1016/S0098-3004(97)00137-4
[16] J. Kusuma, R.G. Balakrishna. Solar Energy, **159** (1), 682–696 (2018). DOI: 10.1016/j.solener.2017.11.037
[17] H.J. Snaith, M. Grätzel. Adv. Mater., **18**, 1910 (2006).
[18] E. Hendry, M. Koeberg, B. O'Regan, M. Bonn. Nano Lett., **6** (4), 755–759 (2006). DOI: 10.1021/nl0600225
[19] A.A. Logunov, A.I. Mashin, I.Yu. Stroganov. Fiz. Tekh. Poluprovodn., **48** (5), 702–705 (2014).
[20] D. Bartolomeo. Phys. Rep., **606**, 1–58 (2016). DOI: 10.1016/j.physrep.2015.10.003

Translated by D.Safin